Response to Reviewer 1

We sincerely thank Reviewer 1 for taking the time to carefully review our manuscript and provide constructive feedback. The reviewer's comments were highly valuable in identifying areas of improvement, need for clarity, and strengthening the scientific interpretation of our results. In the revised manuscript, Reviewer 1's comments are shown *in **blue***, with our responses provided directly below each comment.

1. ***Line 13 and 149: Although UAV technology offers extremely high-resolution data, it is important to recognize that the TSEB model, like most resistance-based energy balance models, must be applied over an appropriate spatial domain to satisfy its physical assumptions and underlying formulations. Consequently, TSEB cannot be applied at the leaf level; the radiative transfer and turbulent exchange processes on which it depends require the model to be run at spatial resolutions of the order of meters. The 15 cm resolution of multispectral and thermal imagery used for running TSEB may need stronger justification for its selection. Evapotranspiration maps are helpful for irrigation management; however, 15 cm resolution may not be feasible for practical irrigation applications.***

We thank the reviewer for this important comment and fully agree that resistance-based two-source energy balance models such as TSEB are not physically formulated for individual leaves. The aerodynamic resistance and radiative transfer parameterizations in TSEB assume canopy–soil exchange occurs over a representative surface element (typically on the order of meters), as is commonly considered in satellite applications.

In our study, the 15 cm GSD was selected to minimize mixed pixels and allow a more robust discrimination of soil and vegetation fractions (especially under partial canopy cover), which improves the retrieval of key TSEB drivers. This strategy has been used in several UAV TSEB studies that exploit very high resolution imagery primarily to reduce mixed-pixel contamination, while still evaluating and interpreting results at aggregated scales (e.g., Hoffmann et al., 2016; Gómez-Candón et al., 2021; Nassar et al., 2020; Gao et al., 2023; Pintér & Nagy, 2022). In our study, final ET estimates were aggregated to the EC flux footprint scale (~tens of meters), ensuring appropriate spatial comparability. At this aggregated scale, modeled ET showed strong agreement with EC observations, indicating that results remain physically consistent despite the high-resolution inputs.

Finally, we agree that 15 cm resolution is finer than required for practical irrigation operations**,** where management zones are typically defined at coarser resolution. We therefore clarify in the revised manuscript that the 15 cm outputs provide diagnostic value for identifying within field spatial heterogeneity in crop water use and stress development, and that these maps can be readily resampled/aggregated to operational irrigation management units (e.g., irrigation sectors or variable-rate irrigation zones).

Paper improvement:

We have expanded the Methods/Discussion to clarify

- the physical interpretation scale of TSEB
- that high-resolution imagery is used to improve retrieval of canopy/soil fractions and inputs
- that results intended for irrigation practice should be aggregated to coarser management resolutions.

2. *Line 162-163: The radiometric sensor calibration and imagery correction are important for reliable LST data. Cited a reference and explained how the calibration parameters were used in the calibration?*

We expanded Section 2.4.1 to clarify the radiometric correction applied to the FLIR Vue Pro R imagery and added supporting references. Before each flight, the camera radiometric settings were updated using field measurements (emissivity, object distance/flight altitude, air temperature, and relative humidity). These parameters are used in the internal radiometric processing of the camera to correct apparent surface temperature for emissivity and atmospheric effects. We also added citations that document the sensitivity of UAV microbolometer LST to these parameters and the need for careful correction/calibration (Kelly et al., 2019; Han et al., 2020; Virtue et al., 2021). We also clarify that despite these radiometric corrections, bias may remain in uncooled thermal sensors under varying environmental conditions, motivating our subsequent target-based correction procedure.

Paper improvement:

We expanded Section 2.4.1 to

- explain how radiometric correction parameters were applied
- add reference supporting this approach.

3. *Line 174-181: Was a thermal infrared sensor or similar used to measure LST from the ground-based reference targets? Later, it stated that a multiple regression model was developed, but it is unclear how the ground temperature was measured and how the environmental variables were used to generate the model.*

Thank you for the opportunity to clarify. Ground reference temperatures were not measured with a ground thermal camera**.** Instead, during the 2021 season we deployed two reference targets for each flight: (1) a high-emissivity metal "hot" plate and (2) a "cold" water target. Target temperatures were measured at the time of UAV overpass (beginning and ending of each flight) using calibrated contact thermometry (contact probe attached to the back of the plate; immersion probe for the water container). These measurements were used as reference temperatures and compared to the corresponding radiometric temperatures extracted from the UAV thermal imagery over the same targets.

Although radiometric correction parameters (emissivity, distance/altitude, air temperature, RH) were applied in the FLIR Vue Pro R settings, a systematic temperature offset remained and varied with meteorological conditions. Therefore, we developed a multiple linear regression model based on the data collected in 2021 (when the targets were deployed) that relates the temperature difference to on-site air temperature, wind speed, and relative humidity. These predictors were selected because UAV uncooled microbolometers are known to show environment-dependent residual bias, particularly linked to wind and atmospheric conditions (Kelly et al., 2019; Han et al., 2020; Virtue et al., 2021). The fitted regression was then applied to subsequent campaigns (2022-2023) to correct UAV LST without requiring repeated deployment of reference targets for every later flight.

Paper improvement:

- We further clarified the reference targets and how the regression was implemented.
- We corrected the reference number made in the paragraph which was incorrect and now points to the correct figure in the appendix.

4. Line 193: There is a lack of understanding of the terms: 1) fractional vegetation cover, 2) vegetation fractional from the viewing angle, and 3) fraction of green LAI. Also, there is an error in naming the terms throughout the paper; for example, at line 193, fractional vegetation cover was labeled FVC, and equation B1 shows the calculation of the green area index. Similar for line 221.

We thank the reviewer for pointing this out. We agree that our original wording was ambiguous and could be interpreted as conflating three distinct variables that play different roles in TSEB: (1) fractional vegetation cover derived from multispectral imagery, (2) view-angle dependent canopy fraction used for radiative partitioning in TSEB, and (3) the fraction of green LAI used to account for senescence effects. The confusion arose because we used Beer–Lambert-type relationships to derive two LAI related inputs from different sensors (multispectral GAI and LiDAR PAI), while TSEB/pyTSEB also uses a Beer–Lambert relation internally to compute a separate directional canopy fraction (f_c) for radiative partitioning. In addition, the terminology used in the main text around lines 193 and 221, as well as the presentation in Table 1, did not sufficiently distinguish these concepts.

To remove ambiguity, we have harmonized definitions and symbols and clarified how each quantity is obtained and used. In the revised manuscript we now clearly separate and consistently define:

- **Fractional vegetation cover (FVC)**: the areal fraction of ground covered by vegetation when viewed from nadir. We estimate FVC from multispectral imagery (NDVI thresholding), and use FVC only as an intermediate variable to derive GAI via a modified Beer–Lambert relationship calibrated with ground LAI measurements. The use of FVC to LAI conversion via Beer–Lambert-type relationships is common in crop remote sensing (e.g., Ali et al., 2015; Thorp et al., 2010; Jia et al., 2017; Zhang et al., 2019; Yue et al., 2021).

- **Directional canopy fractional cover in TSEB/pyTSEB (f_c):** a view-angle dependent canopy fraction used internally for radiative partitioning between canopy and soil. In pyTSEB, this f_c term is computed from LAI using a Beer–Lambert formulation (in our implementation) and is therefore not equivalent to the nadir FVC derived from multispectral soil–vegetation pixel classification.
- **Fraction of green LAI (f_g)**: the fraction of LAI that is photosynthetically active ("green"). This term is used to account for senescence and avoid treating senescent canopy structure as fully transpiring vegetation. In our workflow, f_g is derived during senescence from the relationship between multispectral GAI and LiDAR PAI (i.e., f_g=GAI/PAI) and is used as the model input controlling canopy activity during senescence.

We also clarify an important implementation detail in pyTSEB, which contributed to potential confusion: f_c can be provided as a user input; however, when LAI is supplied, pyTSEB computes f_c internally from the LAI input using Beer–Lambert extinction. In practice, if both LAI and f_c are provided simultaneously, the internally derived f_c from the LAI input is used for radiative partitioning. For this reason, we intentionally did not prescribe an external f_c in our workflow, and instead allowed pyTSEB to derive f_c consistently from the LAI input (GAI or PAI). We have now clarified this explicitly in the revised Methods and Table 1. Finally, we clarify that using different LAI-type inputs (multispectral -derived GAI vs LiDAR-derived PAI) affects not only the canopy structure input itself, but also the internally computed f_c used for radiative partitioning.

***Paper improvements**:*

- Clarified in the Methods (Section 2.4.4) and Table 1 that f_c is computed internally by pyTSEB from LAI (GAI/PAI) and is not derived from MS soil–vegetation pixel classification in our workflow.
- Standardized terminology and symbols for multispectral FVC, internal TSEB directional canopy fraction f_c, and fraction of green LAI (f_g) throughout the manuscript, including around lines 193 and 221.
- Revised Table 1, Fig. 4, and Appendix descriptions to clearly distinguish MS-derived FVC from directional f_c and to better align with the original TSEB formulation and pyTSEB implementation.

We believe these revisions remove the ambiguity and make it clear that FVC in our workflow is not the same as f_c in the TSEB equations, even though both rely on Beer–Lambert concept.

4b. ***Table 1 shows the model input; however, the fractional cover listed in equation (A10) is based on vegetation fractional cover viewed from an angle, which differs from the fractional cover calculated from multispectral data using soil and canopy pixel classification. Revise the original paper of TSEB formulation. Figure 4 shows equation A10, which is not related to the PT equation***

We thank the reviewer for pointing this out. We agree that the original manuscript contained inconsistent equation numbering and cross-referencing between Table 1, Figure 4, and Appendix A, which created confusion regarding the interpretation of f_c and its relation to radiometric temperature and the Priestley–Taylor (PT) formulation.

In the original submission, Eq. A10 was incorrectly used for multiple different terms**:** Table 1 referenced f_c as Eq. A10, Figure 4 linked Eq. A10 to the Priestley–Taylor term, and Appendix A used Eq. A10 for the observed directional radiometric temperature TRAD. This mislabeling contributed to confusion.

We have now corrected the equation numbering and labeling consistently throughout the manuscript. In the revised Appendix A, f_c (directional canopy fraction) is now correctly defined in Eqs. A12–A13, and Table 1 has been updated to reference these equations accordingly. The observed directional radiometric temperature TRAD is now consistently labeled as Eq. A10 (previously A9 in Figure 4), and the Priestley–Taylor formulation is now consistently labeled as Eq. A11 (previously mis-referenced as A10). Figure 4 and all Appendix cross-references have been updated to reflect these corrections.

Paper improvement:

- The misalignment in equation numbering that caused incorrect cross-referencing has been corrected. This has been corrected throughout Appendix A, Figure 4, and Table 1.

5. ***Line 362: TSEB model compute the surface energy fluxes Rn, H, G and LE or ET is calculated as a residual from the energy balance, in order to evaluate the outputs from TSEB model it is also necessary to compare the modeled and measured Rn, H and G. Additionally, TSEB model output are based on closed energy balance and EC data are non-closed energy balance it is recommended to compare for both scenarios: energy balance closed and non-closed.***

Our original focus was on ET because it is the primary variable for water-use monitoring and several recent UAV TSEB studies had validated LE/ET alone (Tunca 2023; De Lima 2024; Pintér & Nagy 2022). However, we agree that assessing the full set of energy fluxes improves transparency. We have therefore updated the revised manuscript to include direct comparisons of modeled versus EC-derived net radiation (Rn), sensible heat flux (H), and ground heat flux (G), and we now present validation results using both open and closed energy-balance EC fluxes.

Energy balance closure was performed using the Bowen-ratio-preserving correction following Twine et al. (2000), consistent with approaches commonly used in comparable UAV TSEB studies (e.g., Hoffmann et al., 2016; Brenner et al., 2017, 2018; Weit et al., 2023; Gao et al., 2023). We initially emphasized comparisons against open EC fluxes to avoid introducing closure-related assumptions (Mokhtari et al., 2021; Nassar et al., 2021), but now provide both open and closed comparisons for completeness.

We provide these plots at the end of this response in Figure R1 – R4 for quick reference. These figures will be further added to the manuscript with minor edits to match formatting.

Paper improvement:

The revised manuscript now reports performance metrics and figures using both open and closed EC fluxes, including:

- Figure R1 modeled versus measured flux scatter plots for the different LST inputs
- Figure R2 RMSE and R^2 bar plot results of different LST inputs when compared against closed EC fluxes
- Figure R3 modeled versus measured flux scatter plots for the different LAI inputs
- Figure R4 RMSE and R^2 bar plot results of different LAI inputs when compared against closed EC fluxes

5b. ***The crop water stress can be derived from TSEB outputs. The paper does not present a method for assessing crop water stress.The following paper explains a method to get CWSI from TSEB:*** **https://doi.org/10.1016/j.jag.2025.104737***. Assessment of different remote sensing techniques to estimate the CWSI of almond trees using canopy temperature.*

We thank the reviewer for this valuable suggestion. We agree that UAV-derived TSEB outputs can be used not only to estimate evapotranspiration (ET), but also to derive spatial indicators of crop water stress. In the original manuscript, we focused primarily on the reliability of UAV–TSEB ET estimates (input retrieval, calibration, and validation against EC). Nevertheless, potential water-deficit areas could already be identified from within-field spatial variability in ET during each flight, where locally reduced ET indicated reduced canopy water use relative to adjacent high-ET zones. These patterns were consistent with later observed reductions in multispectral greenness and LiDAR-derived canopy density, supporting the utility of thermal-based ET mapping for early detection of emerging stress signals.

We have expanded the revised Discussion to more explicitly describe how TSEB outputs can support crop water stress monitoring. In particular, integrating rainfall/soil moisture information and hourly to daily scaling can improve stress quantification. We now also cite and discuss recent work demonstrating how thermal stress indices such as the Crop Water

Stress Index (CWSI) can be derived from TSEB outputs using temperature and energy balance constraints (including the study suggested by the reviewer).

In addition, we have now included a daily ET upscaling component using the approach evaluated by Cammalleri et al. (2014), which has also been applied and tested in UAV based contexts (e.g., Nassar et al., 2021). Using our best-performing UAV TSEB configuration, we now generate daily ET estimates and directly compare them with EC daily ET, reported for both open and closed conditions. We additionally include a daily-scale stress proxy by presenting daily ET relative to FAO-56 reference/potential ET (K_s) which highlights spatial and seasonal patterns of water deficit conditions.

Paper improvements:

- Clarified that the current study focuses on instantaneous ET accuracy and model-input optimization but discuss how they should be interrelated into daily ET amounts to support irrigation and crop stress detection efforts.
- Added a paragraph to the Discussion explaining how spatial ET patterns indicate potential water stress and how TSEB outputs could support CWSI derivation.
- Added a figure (Figure R5 in "New Figures" at the end of this response)

6. ***Line 545: A Daily ET map is needed for irrigation scheduling, and an extrapolation technique using weather data can be used to upscale from hourly to daily ET. However, soil moisture and rainfall data are required for irrigation scheduling. In the literature, extrapolation techniques were assessed for ET derived from UAV data.***

We thank the reviewer for this important point and agree that daily ET estimates are required for many agronomic applications (e.g., irrigation scheduling), and that several methods exist to temporally upscale high-resolution UAV ET snapshots to daily time series. In the original manuscript, our primary objective was to evaluate the accuracy and sensitivity of UAV TSEB ET estimates on flight days, focusing on calibration, input uncertainty, and validation against eddy covariance fluxes. This focused on improving the direct calculation of instantaneous ET using UAV multi-sensor inputs (thermal, multispectral, LiDAR) and evaluating these outputs against 1-hour averaged eddy covariance (EC) fluxes. This approach isolates the effects of model inputs, surface temperature, LAI, and the fraction of green LAI (f_g), on the accuracy of ET itself, without adding uncertainty from temporal upscaling or cumulative stress metrics.

To better address the reviewer's comment, we have expanded the Discussion to explicitly reference established temporal upscaling approaches that combine UAV ET with meteorological forcing and/or reference ET for daily scaling and gap filling (e.g., Sánchez et al., 2019; Brenner et al., 2017; Pintér & Nagy, 2022). In addition, we now include a new figure showing daily UAV TSEB ET trajectories throughout each growing season , compared against EC daily ET (open and closed energy balance) and FAO-56

potential/reference ET, thereby illustrating how UAV ET snapshots can be integrated into a daily ET framework.

Paper improvements:

- Added a paragraph to the Discussion explaining the rationale for using instantaneous ET validation and its implications for daily scaling.
- Added citations to studies addressing temporal upscaling/daily ET interpolation to better contextualize UAV ET mapping within daily ET applications.
- Added a new figure in the revised manuscript demonstrating daily ET interpolation from instantaneous UAV acquisitions and seasonal dynamics (Figure R5 in "New Figures" at the end of this document)

7. *Using high-resolution UAV imagery allows for canopy and soil temperature pixel separation. TSEB-2T, using canopy and soil temperatures, reported better results than TSEB-PT. TSEB-2 T does not consider Priestley-Taylor formulation initialization. Why was the criterion to use TSEB-PT having high-resolution imagery?*

We thank the reviewer for raising this point. The TSEB-2T configuration explicitly separates canopy and soil temperatures, which can be advantageous when thermal imagery allows a reliable separation of canopy and soil components (e.g., sparse canopies with substantial soil exposure). However, comparative studies report mixed results regarding the relative performance of TSEB-2T versus TSEB-PT, with only marginal or inconsistent improvements depending on canopy structure and conditions (e.g., Nieto et al., 2019; Guzinski et al., 2020; Gao et al., 2023). In practice, TSEB-2T is most often applied to vineyards/orchards or other sparse canopies where soil contributions remain significant.

In our study, we initially evaluated both TSEB-2T and TSEB-PT for the 2021 campaign. We found that TSEB-2T slightly improved ET estimation during early-stage sugar beet conditions when canopy cover was sparse. However, as canopy closure increased, the improvement was not consistent and in some cases performance deteriorated relative to TSEB-PT. Given the highly dynamic canopy development of sugar beet and potato, and the near-complete canopy cover of winter wheat for most of the season, the TSEB-PT configuration proved more stable and robust across crop stages.

Moreover, TSEB-PT is more widely adopted in UAV and satellite use cases and provides a well-established framework for sensitivity evaluation of key UAV-derived inputs (e.g., LST, LAI, and f_g) which is the main focus of this study. The model's internal canopy/soil partitioning (through LAI and (f_c) extinction-based radiative partitioning and iterative resistance constraints) enables consistent flux estimation across partial to full canopy cover conditions.

Thus, our decision to use TSEB-PT was guided by its proven stability across varying canopy structures, broad applicability across crops, and interpretability for testing high-resolution UAV input datasets (LiDAR, multispectral, and thermal). Nevertheless, we acknowledge that for canopies with persistent soil exposure (e.g., vineyards, orchards),

TSEB-2T may offer advantages, as also discussed in Gao et al. (2023). This rationale and supporting references have been added to the revised manuscript.

Paper improvements:

- Added to the introduction and discussion with mentioned citations about possible improvements with TSEB-2T with vegetation with large and/or consistent soil exposure.
- Added explanation in introduction to why TSEB-PT was chosen over TSEB-2T in this use case but that there could be benefits to using TSEB-2T in other cases.

8. *How was the shadow managed in the multispectral and thermal imagery, and how was the impact on TSEB results?*

We acknowledge that cast shadows can influence both thermal and multispectral UAV products, particularly in heterogeneous or vertically structured canopies (e.g., orchards and vineyards) and under low solar elevation angles (Aboutalebi et al., 2019; Lu et al., 2022; Gao et al., 2023). In our study, however, shadow effects were expected to be limited because crop height was relatively low (≤0.6 m for sugar beet and potato), and winter wheat reached dense canopy closure during later stages. Under these conditions, shading has a smaller impact on the observed top-of-canopy radiometric temperature and vegetation reflectance compared to tall, discontinuous canopies.

For the thermal imagery, we note that UAV measurements represent an instantaneous canopy temperature snapshot that inherently includes local sunlit/shaded conditions. This may become more critical when temporally upscaling to daily ET (since shadow positions shift throughout the day). However, our primary evaluation focuses on instantaneous ET (hourly EC comparison around overpass), where such temporal shadow dynamics are less influential. For multispectral imagery, shadows can affect soil–vegetation discrimination and spatial LAI/GAI estimates, but this impact was minimized by conducting flights under relatively high solar angles and over homogeneous crop canopies.

Importantly, the LiDAR structural LAI/PAI is independent of illumination conditions and therefore not affected by shading, representing an additional advantage of the multi-sensor approach, particularly under conditions where multispectral canopy retrievals may be shadow biased.

We have added a short discussion to explicitly acknowledge the potential impact of shadows on UAV thermal and multispectral products, and to note that explicit shadow/sunlit separation or bidirectional correction may be more critical for taller, discontinuous canopies (e.g., vineyards/orchards) and for daily ET upscaling applications (Aboutalebi et al., 2019; Gao et al., 2023).

Paper improvements:

- We added a short section describing shadow effects and mitigation strategies in the UAV processing workflow, and clarified how residual shadow related uncertainty may affect multispectral and thermal data.

Minor Comments

- ***Line 42: The citation is missing a parenthesis***
  - The missing parenthesis has been added.

- ***Line 115: Adding the flux footprint of the EC tower may explain the predominant winds on the study site***
  - The flux footprint reference has been updated in the main text and now correctly points to its location in the Appendix.

- ***Line 236: Net radiation (Rn) is not the same as incoming solar radiation; line 147 shows incoming solar radiation as Rn***
  - The misuse of "Rn" to refer to incoming shortwave radiation has been corrected.

- ***Line 293: there is no plot b) correlation of weather conditions with the difference (delta) between the thermal sensor and actual temperature of ground thermal targets for each date.***
  - The text now correctly cites the relocated Appendix figure.

New Paper Figures

This document provides additional figures generated for the revision, including (i) expanded validation against open and energy-balance-closed eddy covariance (EC) fluxes for all energy balance components, (ii) sensitivity comparisons for land surface temperature (LST) and LAI/green fraction parameterizations, and (iii) daily ET upscaling and stress proxy analysis.

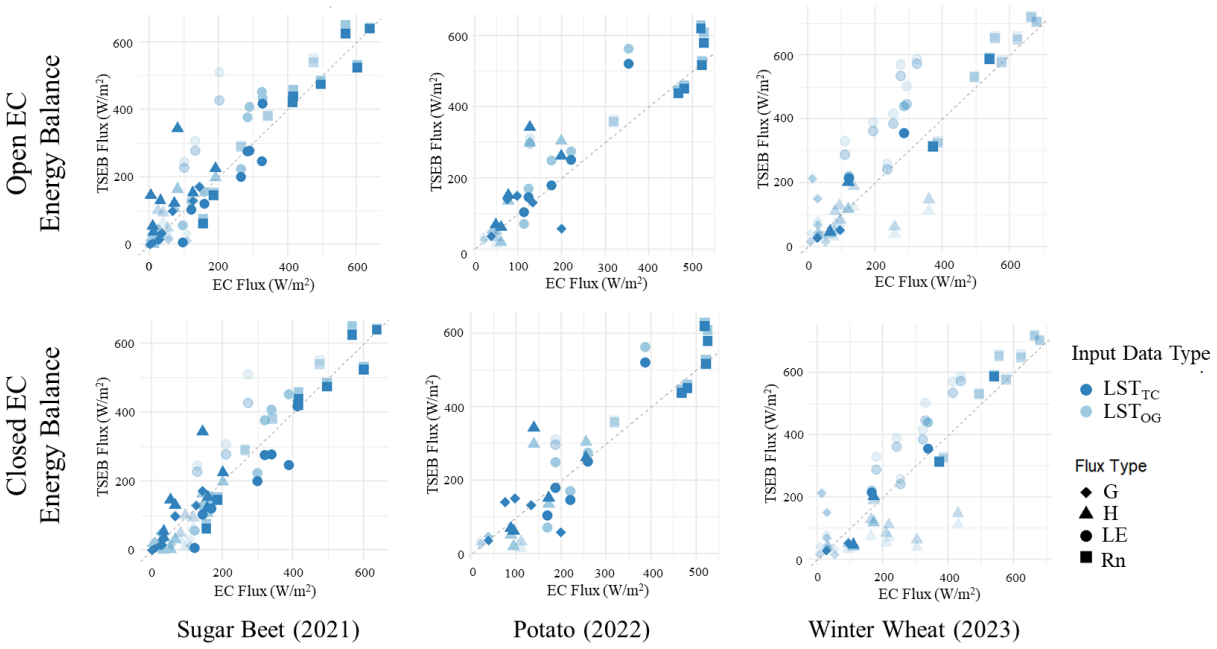

Figure R1. Comparison of modeled TSEB fluxes against eddy covariance (EC) flux observations for each crop season. The upper panels show comparisons using **open** EC energy balance fluxes, while the lower panels show comparisons using **closed** EC energy balance fluxes obtained with the Bowen-ratio-preserving correction. The colors indicate the two land surface temperature inputs while the shapes indicate the different fluxes. Shaded points represent observations acquired during the defined crop senescence period.

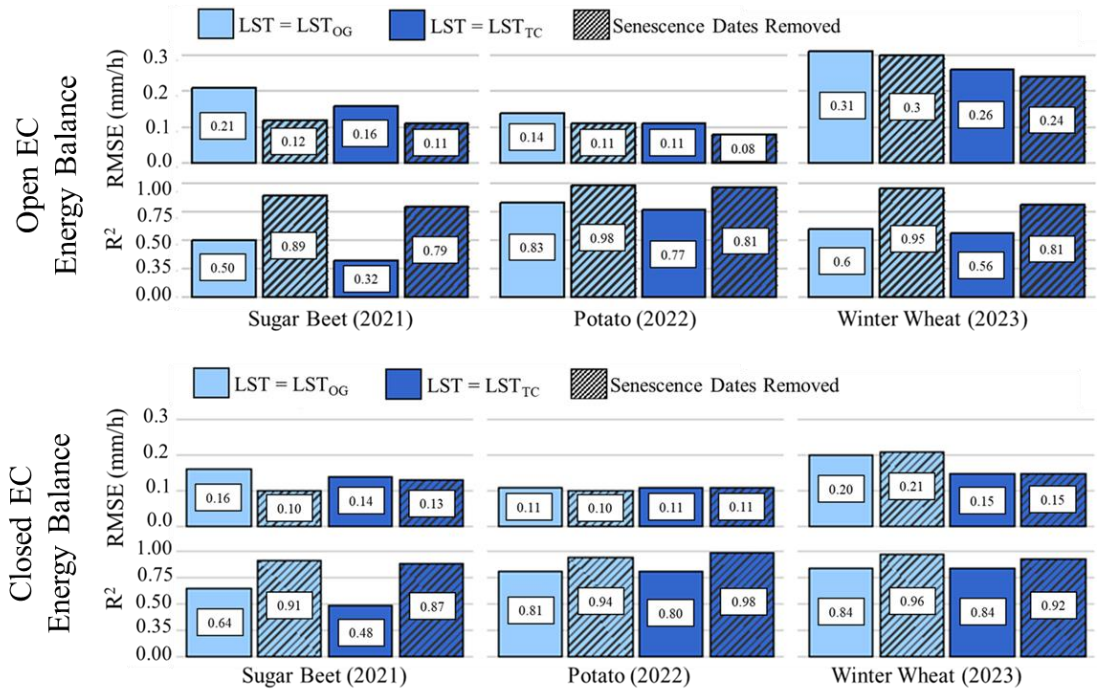

Figure R2. RMSE and R^2 between modeled TSEB-PT ET and EC derived ET, open and closed energy balances, averaged over the EC flux footprint. Two TSEB-PT model runs are compared based on land surface temperature (LST) input: original (OG) and target corrected (TC). Statistical metrics are presented for the entire growing season and excluding senescence periods, highlighting the influence of canopy condition on model performance.

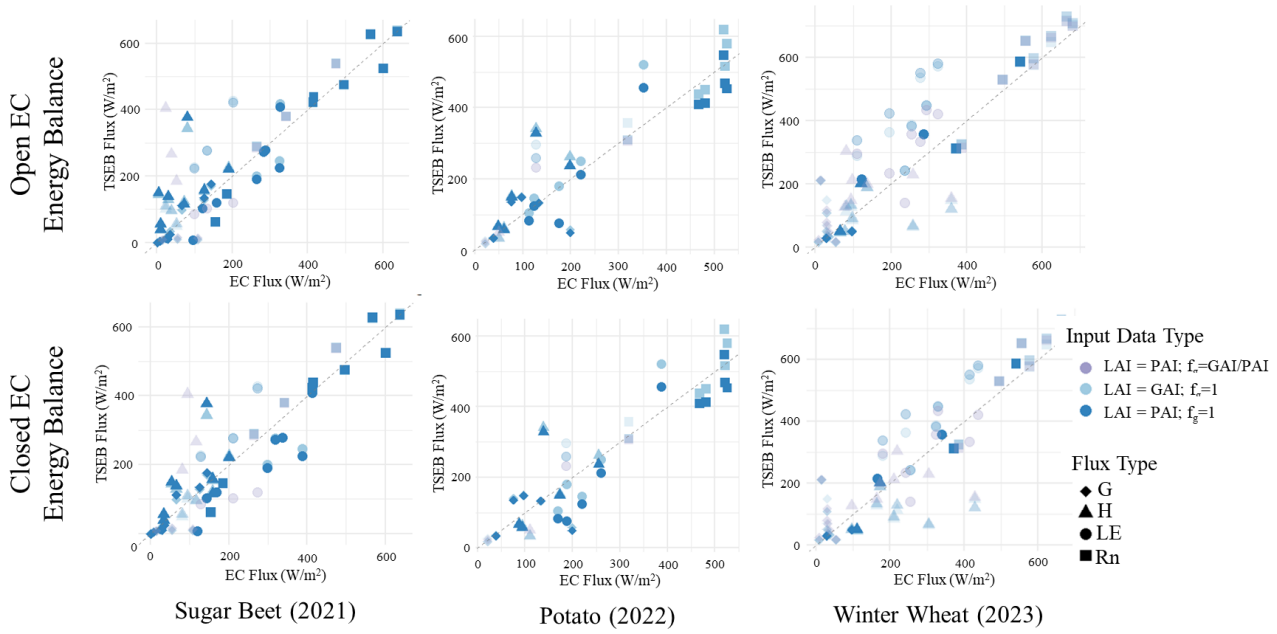

Figure R3. Comparison of modeled TSEB energy balance fluxes against eddy covariance (EC) observations for each crop season under different UAV derived vegetation parameter configurations (LAI inputs and fraction of green LAI). The upper panels show comparisons using **open** EC fluxes, while the lower panels show comparisons using **closed energy balance** EC fluxes obtained with a Bowen-ratio-preserving correction. Colors indicate the LAI/f_g configurations, while marker shapes distinguish the individual flux components. Lighter markers represent observations acquired during the defined crop senescence period.

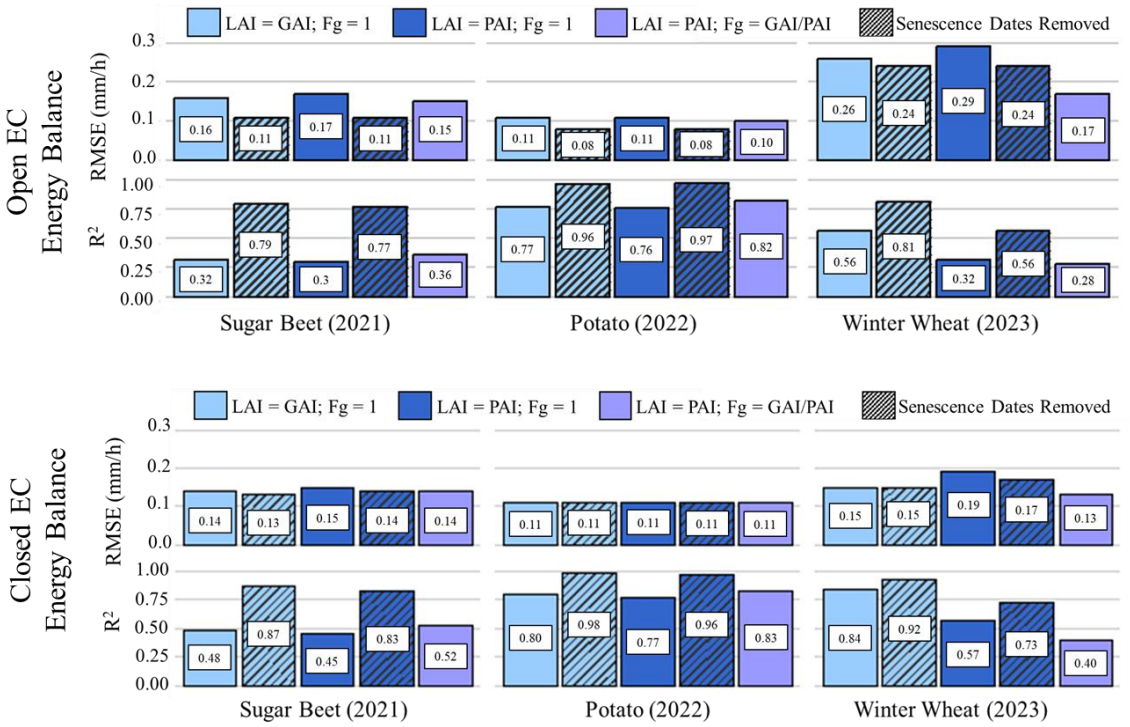

Figure R4. RMSE and R^2 between TSEB-PT modeled ET and EC derived ET, open and closed energy balances, averaged over the EC flux footprint. Two different LAI inputs were evaluated: green area index (GAI) and plant area index (PAI). Statistical metrics are shown for all campaign dates and separately for dates excluding senescence. During senescence periods, a third approach using the fraction of green LAI (fg = GAI/PAI) was also evaluated to scale transpiration according to functional canopy condition.

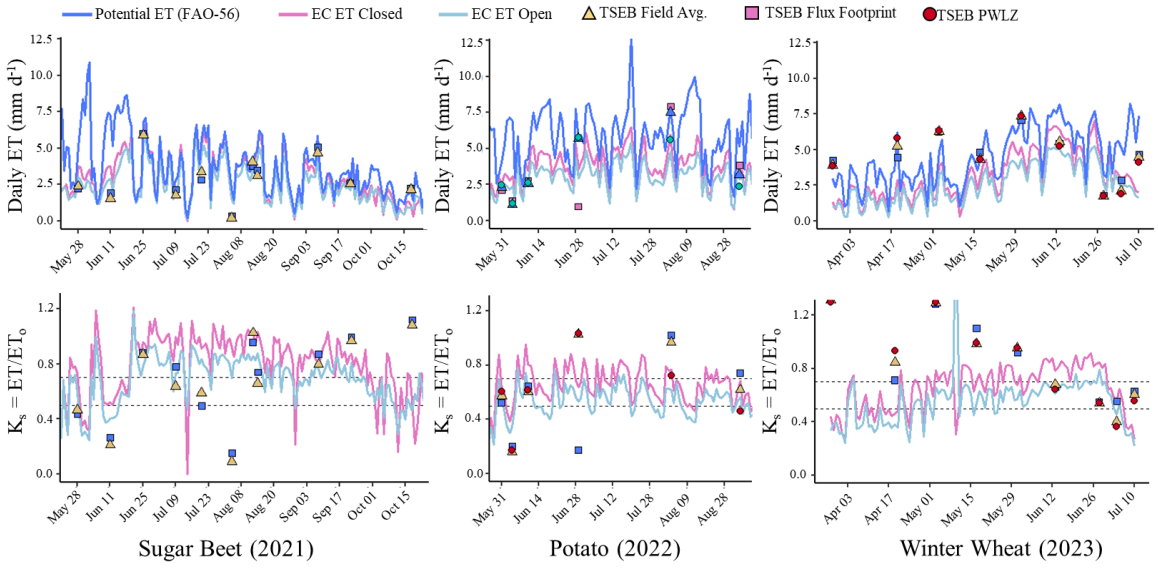

Figure R5. Daily evapotranspiration (ET) time series and daily-scale stress proxy derived from UAV–TSEB and EC measurements. **Top panels:** interpolated daily ET from UAV acquisition compared against EC daily ET (open and closed energy balances) and FAO-56 reference/potential ET. **Bottom panels:** corresponding relative ET stress proxy (K_s) computed as the ratio of daily actual ET to FAO-56 reference/potential ET, illustrating seasonal development of water deficit conditions across crops. Horizontal dashed lines represent 0.7 possible water stress and 0.5 likely water stress compared to atmospheric demand. The different shapes depict different spatial domains of pixel averages from the UAV instantaneous UAV ET that is then upscaled to daily it with including TSEB field average, the flux footprint weighted average, and the average within the potential water limitation zones (PWLZ) from figures 14 and 15.

References:

Aboutalebi, M., Torres-Rua, A. F., McKee, M., Nieto, H., Kustas, W., & Coopmans, C. (2019). The impact of shadows on partitioning of radiometric temperature to canopy and soil temperature based on the contextual two-source energy balance model (TSEB-2T). *Proceedings of SPIE--the International Society for Optical Engineering, 11008.* https://doi.org/10.1117/12.2519685

Ali, M., Montzka, C., Stadler, A., Menz, G., Thonfeld, F., & Vereecken, H. (2015). Estimation and Validation of RapidEye-Based Time-Series of Leaf Area Index for Winter Wheat in the Rur Catchment (Germany). *Remote Sensing*, *7*(3), Article 3. https://doi.org/10.3390/rs70302808

Brenner, C., Thiem, C. E., Wizemann, H.-D., Bernhardt, M., & Schulz, K. (2017). Estimating spatially distributed turbulent heat fluxes from high-resolution thermal imagery acquired with a UAV system. *International Journal of Remote Sensing*, *38*(8–10), 3003–3026. https://doi.org/10.1080/01431161.2017.1280202

Brenner, C., Zeeman, M., Bernhardt, M., & Schulz, K. (2018). Estimation of evapotranspiration of temperate grassland based on high-resolution thermal and visible range imagery from unmanned aerial systems. *International Journal of Remote Sensing*, *39*(15–16), 5141–5174.

Cammalleri, C., Anderson, M.C., Kustas, W.P. (2014). Upscaling of evapotranspiration fluxes from instantaneous to daytime scales for thermal remote sensing applications. Hydrol. Earth Syst. Sci. 18, 1885–1894

de Lima, G. S. A., Ferreira, M. E., Sales, J. C., de Souza Passos, J., Maggiotto, S. R., Madari, B. E., de Melo Carvalho, M. T., & de Almeida Machado, P. L. O. (2024). Evapotranspiration measurements in pasture, crops, and native Brazilian Cerrado based on UAV-borne multispectral sensor. *Environmental Monitoring and Assessment, 196*(11), 1105. https://doi.org/10.1007/s10661-024-13224-7

Gao, R., Torres-Rua, A. F., Nieto, H., Zahn, E., Hipps, L., Kustas, W. P., Alsina, M. M., Bambach, N., Castro, S. J., Prueger, J. H., Alfieri, J., McKee, L. G., White, W. A., Gao, F., McElrone, A. J., Anderson, M., Knipper, K., Coopmans, C., Gowing, I., … Dokoozlian, N. (2023). ET Partitioning Assessment Using the TSEB Model and sUAS Information across California Central Valley Vineyards. *Remote Sensing, 15*(3), 756.

Gómez-Candón, D., Bellvert, J., & Royo, C. (2021). Performance of the Two-Source Energy Balance (TSEB) Model as a Tool for Monitoring the Response of Durum Wheat to Drought by High-Throughput Field Phenotyping. *Frontiers in Plant Science, 12.*

Guzinski, R., Nieto, H., Sandholt, I., & Karamitilios, G. (2020). Modelling High-Resolution Actual Evapotranspiration through Sentinel-2 and Sentinel-3 Data Fusion. *Remote Sensing, 12*(9), Article 9. https://doi.org/10.3390/rs12091433

Han, X., Thomasson, J. A., Swaminathan, V., Wang, T., Siegfried, J., Raman, R., Rajan, N., & Neely, H. (2020). Field-Based Calibration of Unmanned Aerial Vehicle Thermal Infrared Imagery with Temperature-Controlled References. *Sensors, 20*(24), Article 24.

Hoffmann, H., Nieto, H., Jensen, R., Guzinski, R., Zarco-Tejada, P., & Friborg, T. (2016). Estimating evaporation with thermal UAV data and two-source energy balance models. *Hydrology and Earth System Sciences, 20*(2), 697–713.

Jia, K., Li, Y., Liang, S., Wei, X., & Yao, Y. (2017). Combining Estimation of Green Vegetation Fraction in an Arid Region from Landsat 7 ETM+ Data. *Remote Sensing, 9*(11), Article 11. https://doi.org/10.3390/rs9111121

Kelly, J., Kljun, N., Olsson, P.-O., Mihai, L., Liljeblad, B., Weslien, P., Klemedtsson, L., & Eklundh, L. (2019). Challenges and Best Practices for Deriving Temperature Data from an Uncalibrated UAV Thermal Infrared Camera. *Remote Sensing, 11*(5), Article 5.

Lu, S., Xuan, J., Zhang, T., Bai, X., Tian, F., & Ortega-Farias, S. (2022). Effect of the Shadow Pixels on Evapotranspiration Inversion of Vineyard: A High-Resolution UAV-Based and Ground-Based Remote Sensing Measurements. *Remote Sensing, 14*(9), Article 9. https://doi.org/10.3390/rs14092259

Mokhtari, A., Ahmadi, A., Daccache, A., & Drechsler, K. (2021). Actual Evapotranspiration from UAV Images: A Multi-Sensor Data Fusion Approach. *Remote Sensing, 13*(12), Article 12. https://doi.org/10.3390/rs13122315

Nassar, A., Torres-Rua, A., Kustas, W., Nieto, H., McKee, M., Hipps, L., Stevens, D., Alfieri, J., Alsina, M., McKee, L., Coopmans, C., Sanchez, L., & Dokoozlian, N. (2020). Influence of Model Grid Size on the Estimation of Surface Fluxes Using the Two Source Energy Balance Model and sUAS Imagery in Vineyards. *Remote Sensing, 12*, 342.

Nassar, A., Torres-Rua, A., Kustas, W., Alfieri, J., Hipps, L., Prueger, J., Nieto, H., Alsina, M. M., White, W., McKee, L., Coopmans, C., Sanchez, L., & Dokoozlian, N. (2021). Assessing Daily Evapotranspiration Methodologies from One-Time-of-Day sUAS and EC Information in the GRAPEX Project. *Remote Sensing, 13*(15), Article 15. https://doi.org/10.3390/rs13152887

Nieto, H., Kustas, W. P., Torres-Rúa, A., Alfieri, J. G., Gao, F., Anderson, M. C., White, W. A., Song, L., Alsina, M. del M., Prueger, J. H., McKee, M., Elarab, M., & McKee, L. G. (2019). Evaluation of TSEB turbulent fluxes using different methods for the retrieval of soil and canopy component temperatures from UAV thermal and multispectral imagery. *Irrigation Science, 37*(3), 389–406.

Pintér, K., & Nagy, Z. (2022). Building a UAV Based System to Acquire High Spatial Resolution Thermal Imagery for Energy Balance Modelling. *Sensors, 22*(9), Article 9. https://doi.org/10.3390/s22093251

Sánchez, J. M., López-Urrea, R., Valentín, F., Caselles, V., & Galve, J. M. (2019). Lysimeter assessment of the Simplified Two-Source Energy Balance model and eddy covariance system to estimate vineyard evapotranspiration. *Agricultural and Forest Meteorology, 274*, 172–183. https://doi.org/10.1016/j.agrformet.2019.05.006

Thorp, K. R., Hunsaker, D. J., & French, A. N. (2010). Assimilating Leaf Area Index Estimates from Remote Sensing into the Simulations of a Cropping Systems Model. *Transactions of the ASABE, 53*(1), 251–262. https://doi.org/10.13031/2013.29490

Tunca, E. (2023). Evaluating the performance of the TSEB model for sorghum evapotranspiration estimation using time series UAV imagery. *Irrigation Science, 42*(5), 977–994. https://doi.org/10.1007/s00271-023-00887-2

Twine, T. E., Kustas, W. P., Norman, J. M., Cook, D. R., Houser, P. R., Meyers, T. P., Prueger, J. H., Starks, P. J., & Wesely, M. L. (2000). Correcting eddy-covariance flux underestimates over a grassland. *Agricultural and Forest Meteorology, 103*(3), 279–300. https://doi.org/10.1016/S0168-1923(00)00123-4

Virtue, J., Turner, D., Williams, G., Zeliadt, S., McCabe, M., & Lucieer, A. (2021). Thermal Sensor Calibration for Unmanned Aerial Systems Using an External Heated Shutter. *Drones, 5*(4), Article 4.

Wei, J., Dong, W., Liu, S., Song, L., Zhou, J., Xu, Z., Wang, Z., Xu, T., He, X., & Sun, J. (2023)**.** Mapping super high resolution evapotranspiration in oasis-desert areas using UAV

multi-sensor data. *Agricultural Water Management, 287*, 108466. https://doi.org/10.1016/j.agwat.2023.108466

Yue, J., Guo, W., Yang, G., Zhou, C., Feng, H., & Qiao, H. (2021). Method for accurate multi-growth-stage estimation of fractional vegetation cover using unmanned aerial vehicle remote sensing. *Plant Methods, 17*(1), 51. https://doi.org/10.1186/s13007-021-00752-3

Zhang, L., Zhang, H., Niu, Y., & Han, W. (2019). Mapping Maize Water Stress Based on UAV Multispectral Remote Sensing. *Remote Sensing, 11*(6), Article 6. https://doi.org/10.3390/rs11060605

Zhang, S., Chen, H., Fu, Y., Niu, H., Yang, Y., & Zhang, B. (2019). Fractional Vegetation Cover Estimation of Different Vegetation Types in the Qaidam Basin. *Sustainability, 11*(3), Article 3. https://doi.org/10.3390/su11030864